Catalysis Today 376 (2021) 311–317

Contents lists available at ScienceDirect

Catalysis Today

journal homepage: www.elsevier.com/locate/cattod

Promoting effect of acid sites on NH_3-SCO activity with water vapor participation for Pt-Fe/ZSM-5 catalyst

Fei Wang [a,b,d,1], Ying Zhu [a,c,1], Zhao Li [d], Yulong Shan [b], Wenpo Shan [a,c], Xiaoyan Shi [b], Yunbo Yu [a,b], Changbin Zhang [b], Kai Li [d], Ping Ning [d], Yan Zhang [a,c,*], Hong He [a,b,c,*]

[a] Center for Excellence in Regional Atmospheric Environment, Institute of Urban Environment, Chinese Academy of Sciences, Xiamen 361021, China
[b] State Key Joint Laboratory of Environment Simulation and Pollution Control, Research Center for Eco-Environmental Sciences, Chinese Academy of Sciences, Beijing 100085, China
[c] Zhejiang Key Laboratory of Urban Environmental Processes and Pollution Control, Ningbo Urban Environment Observation and Research Station-NUEORS, Chinese Academy of Sciences, Ningbo 315800, China
[d] Faculty of Environmental Science and Engineering, Kunming University of Science and Technology, Kunming 650500, Yunnan, China

ARTICLE INFO

Keywords:
Ammonia (NH_3)
NH_3-SCO
Diesel exhaust
Pt-Fe/ZSM-5
Acid site

ABSTRACT

Ammonia (NH_3) slip from denitration (deNO_x) process has been increasingly concerned due to the recent findings that NH_3 played an important role in promoting the formation of haze. Considering the high-temperature and humidity application conditions of diesel exhaust and the location of NH_3-SCO system, Pt/Fe/ZSM-5 catalyst was selected. In this work, Pt-Fe/ZSM-5 catalysts with two different Si/Al ratios (25, 50) were prepared through ion-exchange method and the NH_3-SCO activity were compared both in dry and wet (5% H_2O) circumstances. The Si/Al 25 sample exhibited higher intrinsic activity (dry circumstance) than the Si/Al 50 sample. However, with H_2O addition the activity of Si/Al 25 sample decreased dramatically while Si/Al 50 sample maintained higher level. BET, XRD, XPS, H_2-TPR, NH_3-TPD and *in situ* DRIFTS characterization results showed that abundant metallic Pt (Pt°) was beneficial to NH_3-SCO activity, strong acid site determined the water-resisting property of the catalysts during NH_3-SCO with H_2O participation.

1. Introduction

Ammonia (NH_3), mainly emitted from agriculture and animal husbandry, is also a common gas which has been widely used in chemical, light industry, chemical fertilizer, pharmaceutical, synthetic fiber and other fields [1,2]. NH_3 has potentially harmful effects on both human health and the environment. Moreover, it was recently reported that NH_3 greatly contributes to the formation of haze [1,3–5]. In recent years, it has been getting a lot of attention because of the application in deNO_x, in which the selective catalytic reduction (SCR) of NO_x with NH_3 is the most effective method of NO_x purification in mobile and stationary pollution sources at present [1,6]. However, in the NH_3-SCR systems, an enhanced urea injection would be necessitated to reduce the nitrogen oxide emissions, which generating a higher ammonia slip [7]. Therefore, the slipping NH_3 is urgent to control, especially, it has been precisely limited in China VI.

Selective catalytic oxidation of ammonia (NH_3-SCO) is regarded as a highly promising method for NH_3 emission control. Many types of catalysts have been reported to possess high NH_3-SCO activity, such as noble metal catalysts (Pt, Au, Ag or Ir, *etc.*) [8–14], metallic oxide catalysts (CuO, Fe_3O_4, NiO, *etc.*) [15–22] and zeolite catalysts (Cu-ZSM-5, Cu-SSZ-13, Pd-Y, Fe-ZSM-5, Fe-Beta, *etc.*) [7,23–30]. The noble metals including Pt, Ag and Pd have applied as SCO catalysts due to their excellent low-temperature catalytic activity [24,31,32]. Our previous study showed that Ag/nano-Al_2O_3 catalyst was extremely active for NH_3 oxidation at low temperature (T_{90} = 90 ℃) [31]. However, the deactivation of Ag/nano-Al_2O_3 catalyst in the presence of H_2O limited its application, because of the humid real conditions of diesel exhaust. ZSM-5 was selected due to its water resistance, moreover, its several features appeared to be beneficial for NH_3-SCO reaction: high surface area, intrinsic acidity and stability [33]. NH_3-SCO system is located downstream of the SCR catalysts in heavy-loaded diesel automobiles, so

* Corresponding authors at: Center for Excellence in Regional Atmospheric Environment, Institute of Urban Environment, Chinese Academy of Sciences, Xiamen 361021, China.
E-mail addresses: yzhang3@iue.ac.cn (Y. Zhang), honghe@rcees.ac.cn (H. He).
[1] These authors contributed equally to this work.

https://doi.org/10.1016/j.cattod.2020.06.039
Received 28 February 2020; Received in revised form 20 May 2020; Accepted 13 June 2020
Available online 27 June 2020
0920-5861/

the low temperature operation of the SCO is often required. Previous studies reported that ZSM-5 presented high activity for the reaction, achieving 100 % NH_3 conversion and 100 % N_2 selectivity at 400–450 ◦C [34–36]. However, they are significantly less active than supported noble metal catalysts. To ensure low temperature activity, therefore, Pt-Fe/ZSM-5 was selected and prepared as the NH_3-SCO catalyst in this work. In addition, through our previous studies [31,37] acid site was an important factor for the adsorption and activation of NH_3, which thus affected the NH_3-SCO activity. Since Si/Al ratio was reported to have influence on surface acidity of ZSM-5 catalysts [30], the effect of Si/Al ratio on NH_3-SCO activity was studied in this work in both dry and wet circumstances.

In this paper, Pt-Fe/ZSM-5 catalysts with two different Si/Al ratios (25 and 50) were prepared through ion-exchange method, and compared the NH_3-SCO activity in both dry and wet circumstances. The relationship between strong acid site and water-resisting property was then uncovered. Characterization methods such as BET, XRD, XPS, H_2-TPR, NH_3-TPD and *in situ* DRIFTS were used to figure out the effect of Si/Al ratio on physicochemical properties and thus illustrate the structure-function relationship of the catalysts.

2. Experiment

2.1. Catalyst preparation

The catalysts described in this paper were prepared by the ion-exchange method and the active components (Pt 1 wt.%, Fe 1.5 wt.%) were loaded simultaneously on H-ZSM-5 supports with different Si/Al ratios (25, 50). The detailed procedures are as follows: A certain amount of Pt and Fe precursor solutions (H_2PtCl_6 and $FeCl_2$ respectively) were stirred and mixed evenly. The H-ZSM-5 supports with different Si/Al ratios were then impregnated with the mixed solution to incipient wetness. Subsequently, the impregnated samples were loaded into a quartz reactor and exchanged at 650 ℃in flowing N_2 (300 mL/min) for 2 h. After that, the samples were washed with deionized water adequately and dehydration at 120 ℃ overnight. Finally, the obtained samples were calcined at 600 ℃ for 3 h in air and sieved to 40–60 mesh to be used.

2.2. Hydrothermal aging pretreatment

To determine the role of acid sites in water-resisting property of the catalysts during NH_3-SCO reaction, the catalysts were hydrothermal aged in a flow of 10 % H_2O and 90 % air (300 mL/min) at 700 ℃ for 10 h.

2.3. Catalytic activity measurements

The NH_3-SCO activities of the catalysts were measured in a fixed-bed quartz reactor under atmospheric pressure. The reaction conditions were controlled as follows: 25 mg catalysts, 500 ppm NH_3, O_2 10 vol.%, 5% H_2O (when used) and balance N_2. The total flow ratio of the reaction mixture was 100 mL/min with a GHSV of 140,000 h^{-1}.

The concentrations of inlet and outlet NH_3 and NO*x* were continuously monitored with an online FTIR spectrometer (Nicolet is50) equipped with a heated 2 m gas cell and a DTGS detector. Since only NH_3, NO, NO_2 and N_2O were detected in the reaction system, NH_3 conversion (X_{NH3}) and N_2 selectivity (S_{N2}) were calculated as follows:

$$X_{NH3} = \left(1 - \frac{[NH_3]_{out}}{[NH_3]_{in}}\right) \times 100\% \quad (1)$$

$$S_{N2} = \frac{[NH_3]_{in} - [NH_3]out\ \text{-}2[N_2O]_{out}\text{-}[NO_2]_{out}\text{-}[NO]_{out}}{[NH_3]_{in} - [NH_3]out} \times 100\% \quad (2)$$

2.4. Sample characterization

The N_2 adsorption isotherms were detected on a Quantasorb-18 automatic micropore-size analyzer and the specific surface area of the catalysts were then determined by the BET method. The samples were degassed in vacuum at 300 ℃ for 4 h firstly and then adsorbed N_2 at -196 ℃ during the measurements. XRD measurements were conducted with a Bruker D8 ADVANCE Diffractometer with Cu K_α radiation source (λ =0.15406 nm), the 2θ range was 4 to 70° with a scan speed of 6° min^{-1}.

XPS measurement were conducted on a scanning X-ray microprobe (PHI Quantera, ULVAC-PHI, Inc.) with Al K_α radiation. Binding energies of the elements were calibrated with contaminant carbon (C 1s peak, BE = 284.8 eV). H_2-TPR was conducted in a Micromeritics AutoChem II 2920 device, equipped with a CryoCooler and a TCD detector. During H_2-TPR experiments, 100 mg samples were pretreated in 20 % O_2/N_2 (50 mL/min) at 500 ℃ for 30 min and then cooled down to 30 ℃. Prior to the reduction process the samples were purged with Ar for 30 min. Then reduction of the samples was conducted in 10 % H_2/Ar (50 mL/min) flow with the temperature range of 30–700 ℃. The generated H_2O was trapped with the CryoCooler and the H_2 consumption was monitored with the TCD detector.

The acid sites content of the samples was semi-quantitative analyzed with NH_3-TPD method. The experiments were performed with the same apparatus as H_2-TPR except that the signals of NH_3 (m/z = 17) were recorded with a quadrupole mass spectrometer (MKS Cirrus). During the experiments, 100 mg samples were pretreated in 20 % O_2/N_2 flow (50 mL/min) at 500 ℃ for 30 min, and cooled down to 50 ℃. After that, the samples were purged with Ar for another 30 min, and then heated to 700 ℃ with a ratio of 10 ℃/min. The signal was monitored continuously with the MS detector during the desorption process. *In situ* DRIFTS of NH_3 adsorption was further carried out on a Nicolet is50 FTIR spectrometer with an MCT/A detector to detect the acid sites of the catalysts. In the experiment, the spectra were recorded by accumulating 100 scans with a resolution of 4 cm^{-1}.

2.5. DFT calculation

The exchange and correlation energies in this work were described by using the Perdew-Burke-Ernzerhof (PBE) functional [38] with van der Waals correction proposed by Becke-Jonson (*i.e.*, DFT-D3 method) [39] as implemented in the Vienna ab initio simulation package (VASP 5.4.4) [40]. The projector augmented wave method (PAW) was used to describe the electron-ion interaction [41]. The cutoff energy of 400 eV was adopted during the calculations, all atoms of the zeolite and the active site as well as the molecules were fully relaxed until the maximum force on unconstrained atoms was less than 0.02 eV/Å. The 1 × 1×1 k-point grid was adopted based on the Monkhorst-Pack method [33].

Based on previous work [33,42], the structure was modeled using a single unit cell of ZSM-5 zeolite ($Si_{96}O_{192}$) with the cell parameters of a =20.1 Å, b =19.9 Å, and c =13.4 Å. The adsorption energies of H_2O and NH_3 on the zeolite were calculated as follows:

$$E_{ad} = E_{adsorbate+ZSM\text{-}5} - (E_{ZSM\text{-}5} + E_{adsorbate})$$

where $E_{adsorbate+ZSM\text{-}5}$ and $E_{ZSM\text{-}5}$ are the total energies of the adsorbed system and ZSM-5, respectively; and E_{ad} is the adsorption energy of adsorbate on ZSM-5, which can reflect the stability of the adsorbates on the ZSM-5. Negative E_{ad} value means that the adsorption process is exothermic, indicating that corresponding adsorbed state is energetically favorable.

3. Results and discussion

3.1. Catalytic performance

The NH_3-SCO performances of the Pt-Fe/ZSM-5 catalysts with

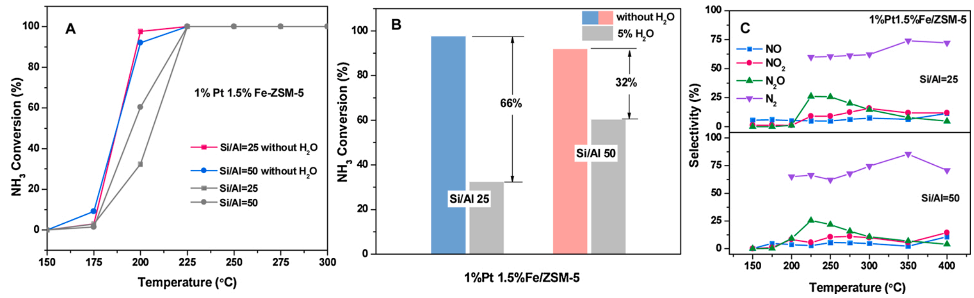

Fig. 1. (A) NH_3-SCO activity over Pt-Fe/ZSM-5 (Si/Al = 25 and 50) samples in dry and wet circumstances at different temperatures. (B) Contrast of NH_3 conversion in dry and wet circumstances at 200 °C. (C) selectivity to N_2, NO, NO_2 and N_2O at different temperatures over Pt-Fe/ZSM-5 (Si/Al rate 25 and 50) samples. Reaction conditions: $[NH_3]$ = 500 ppm, $[O_2]$ = 10 %, $[H_2O]$ = 5 % (when used), balance N_2, total flow ratio = 100 mL/min, GHSV = 140,000 h^{-1}.

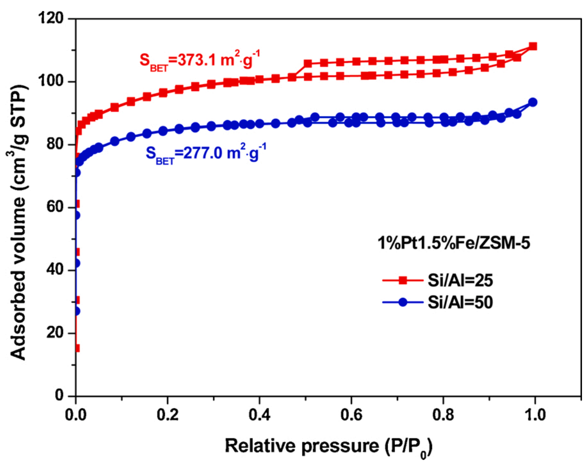

Fig. 2. N_2 adsorption-desorption isotherms of the catalysts.

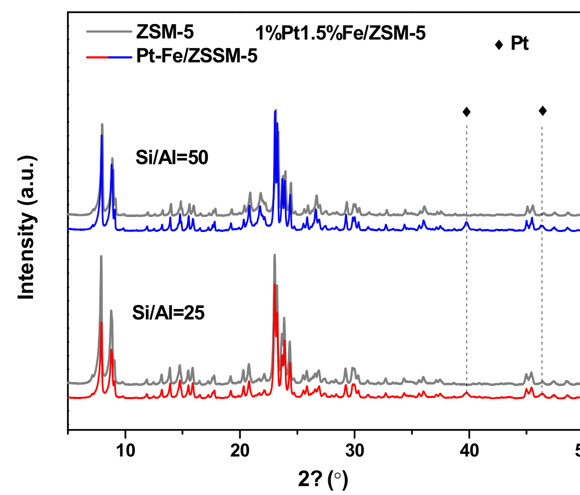

Fig. 3. XRD profiles of pure supports and loaded catalysts.

different Si/Al ratios (25, 50) were tested in dry and wet circumstances with the temperature range of 150–300 °C. As shown in Fig. 1A, the intrinsic activity (dry circumstance) of the two samples were similar, while an inhibiting effect of NH_3-SCO activity had been observed after H_2O addition, which might result from the existence of competition for surface sites between ammonia and water [43]. In addition, only 30 % and over 60 % NH_3 conversion can be observed on Si/Al = 25 and 50 samples, respectively. As shown in Fig. 1B, remarkable decrease of NH_3 conversion occurred after 5% H_2O was introduced on both Si/Al = 25 and 50 samples, while the degree of decline varied greatly on the two samples. On Pt-Fe/ZSM-5 (Si/Al = 25) sample, 66 % NH_3 conversion dropped with the addition of 5% H_2O, while the descent ratio was only 32 % for Pt-Fe/ZSM-5 (Si/Al = 50). Therefore, we concluded that it was the high water-resisting property that resulted in the superior of Pt-Fe/ZSM-5 (Si/Al = 50) in wet circumstance. Fig. 1C presented that the N_2 selectivity maintained in the range of 60–80 % for Si/Al = 25 and 50 samples and showed a rising trend with the temperature going up. The content of NO and NO_2 maintained a low level within the temperature window and N_2O was the main by-product affecting the N_2 selectivity. Since N_2O is just a greenhouse gas, its harmfulness is much lower than that of NO and NO_2, so this level of N_2 selectivity is acceptable in practical applications. Meanwhile, improving N_2 selectivity will be studied in further research.

3.2. Results of characterization

In order to analyze the structure-function relationship of the catalysts and then figure out the reasons of the difference in NH_3-SCO activity and water-resisting property, the catalysts were characterized from structural properties, chemical states and acid sites three aspects, which was confirmed by BET, XRD, XPS, H_2-TPR, NH_3-TPD and *in situ* DRIFTS.

3.2.1. Structural properties

The N_2 adsorption-desorption isotherm and BET surface area of Pt-Fe/ZSM-5 catalysts with different Si/Al ratios were shown in Fig. 2.

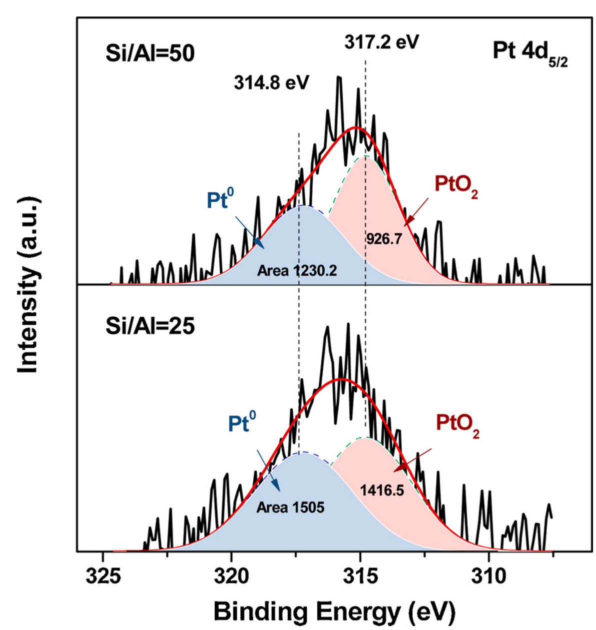

Fig. 4. XPS results of Pt $4d_{5/2}$ profiles of the catalysts.

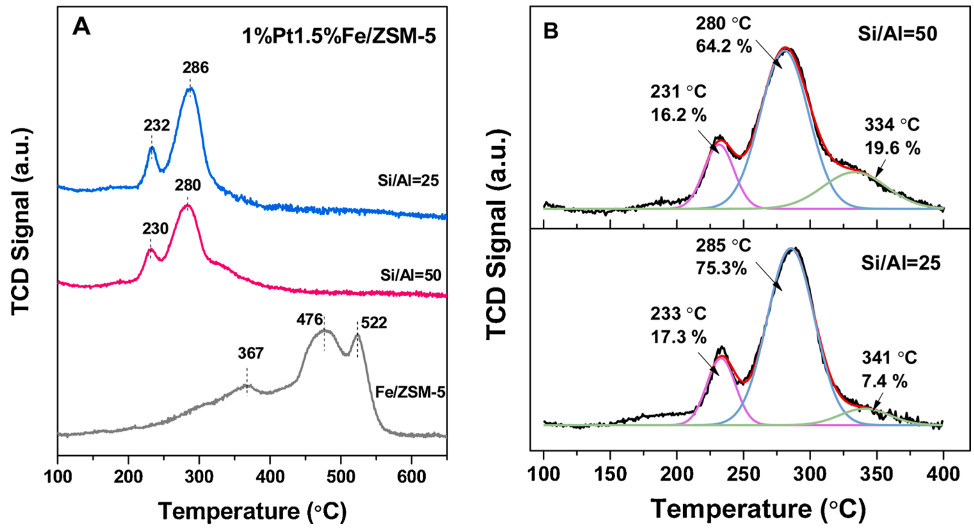

Fig. 5. H_2-TPR profiles of the catalysts.

H4 type of hysteresis loop was presented on Pt-Fe/ZSM-5 catalyst above $P/P_0 = 0.6$ [44], indicated the characteristic of microporous solids [45]. The S_{BET} of Pt-Fe/ZSM-5 (Si/Al = 25) was 373.1 m^2/g, while the S_{BET} of Pt-Fe/ZSM-5 (Si/Al = 50) was 277.0 m^2/g. Combined with the results of NH_3-SCO activity, the BET surface area was not a critical factor.

Fig. 3 showed the XRD patterns of Pt-Fe/ZSM-5 catalysts with different Si/Al ratios, typical MFI peaks of ZSM-5 zeolite were shown at $2\theta = 7.9°$, 8.7°, 23.0° and 23.9° [46] on both samples, coincided with that reported in the literatures [45,47]. Si/Al ratio made little difference for the structure of pure ZSM-5 supports (gray lines in Fig. 3), and the existing state of Pt. The characteristic diffraction peaks of Pt° at 39.8° and 46.2° [48,49] both appeared on Si/Al = 50 and 25 samples. The result indicated that metallic Pt particles were generated on both samples, which may result from the consumption of anchoring sites by Fe.

3.2.2. Chemical states and redox properties

XPS measurement was conducted to investigate the valence state of platinum species in Pt-Fe/ZSM-5 catalysts. Since the energy region of the most intense Pt 4f level (70−80 eV) was overshadowed by Al 2p peak, Pt 4d lines were thus analyzed instead [50]. The asymmetric broad Pt $4d_{5/2}$ (Fig. 4) peaks were deconvoluted into two sub-bands located at 314.8 eV and 317.2 eV, which assigned to Pt° and PtO_2 respectively [50,51]. The presence of Pt° on both samples was consistent with the results of XRD mentioned above. In addition, as shown in Fig. 4, the peak area of Pt° (314.8 eV) in Pt-Fe/ZSM-5 (Si/Al 25) was higher than that in Pt-Fe/ZSM-5 (Si/Al 50), which may due to the aggregation of Pt on Pt-Fe/ZSM-5 (Si/Al 25) to generate more metallic Pt. As presented in HR-TEM and FE-SEM images (Fig. S1 and S2 in the Supporting information). In addition, the trend of Pt° content corresponded with intrinsic activity of the catalysts, confirmed Pt° was the active site for NH_3-SCO on Pt-Fe/ZSM-5 catalysts. This inference was further confirmed by Fig. S3 (in the Supporting information), it was shown that the NH_3-SCO activity of Pt-Fe/ZSM-5 was improved after H_2 reduction especially at low temperatures.

The H_2-TPR profiles of the Pt-Fe/ZSM-5 with different Si/Al ratios and Fe/ZSM-5 catalysts were displayed in Fig. 5. Three H_2 consumption peaks located at 367 ℃, 476 ℃ and 522 ℃ appeared on Fe/ZSM-5 (Fig. 5A). According to the literature [52], the peak at 367 ℃ may be attributed to reduction of Fe_2O_3 to Fe_3O_4, the second one can thus be assigned to subsequent reduction of Fe_4O_3 to metallic Fe. Since the reduction temperature of Fe_2O_3 to metallic Fe is around 530 ℃ [53], the third peak (522 ℃) may result from the subsequent reduction of partial Fe_2O_3 to metallic Fe. Due to the hydrogen overflow on Pt°, the reduction peaks of all the Pt-Fe/ZSM-5 samples transferred to lower temperatures

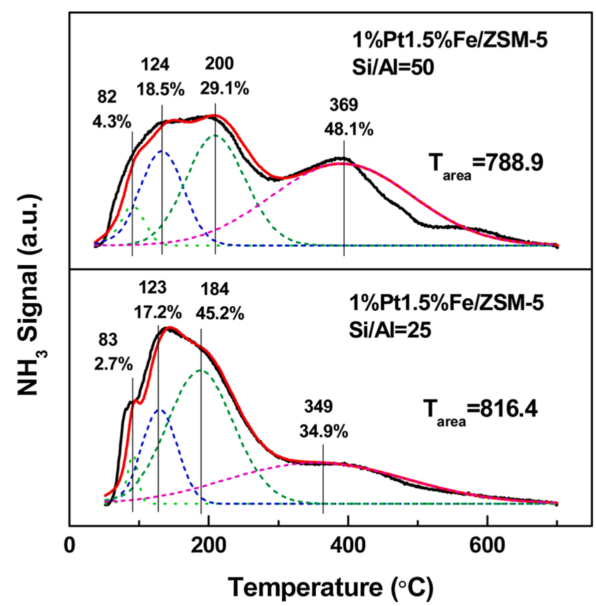

Fig. 6. NH_3-TPD profiles of the catalysts.

compared with Fe/ZSM-5, indicating that the oxidized ability was promoted with the addition of Pt. The profiles of the Pt-Fe/ZSM-5 were fitted into three sub-bands located at around 230, 285 and 335 ℃ as shown in Fig. 5B. The peak at low temperature (230 ℃) mainly assigned to the reduction of PtO_x (*e.g.*, Pt^{4+}→Pt°) [54], the latter two peaks would correspond to the reduction of FeO_x to metallic Fe. The peak at an intermediate temperature (~ 280℃) can be assigned to the iron oxide neighboring the PtOx. The iron oxide was intimately in contact with PtOx, the reduction of which was attributed to the abstraction of O^{2-} by H_2 and facilitated by the presence of platinum [55]. Another peak at *ca.* 335℃ could correspond to the reduction of iron oxide that was remote from the PtOx [55]. It was obvious that the ratio of high-temperature peak (335 ℃) increased (7.4 %→19.6 %) with the enhancement of Si/Al ratio (25→50), indicating the decrease of oxidized ability. This was just consistent with the intrinsic activity of the catalysts. Therefore, combine the results of XPS and H_2-TPR we concluded that the appearance of metallic Pt can improve the oxidized ability of the catalyst and thus enhance the NH_3-SCO intrinsic activity.

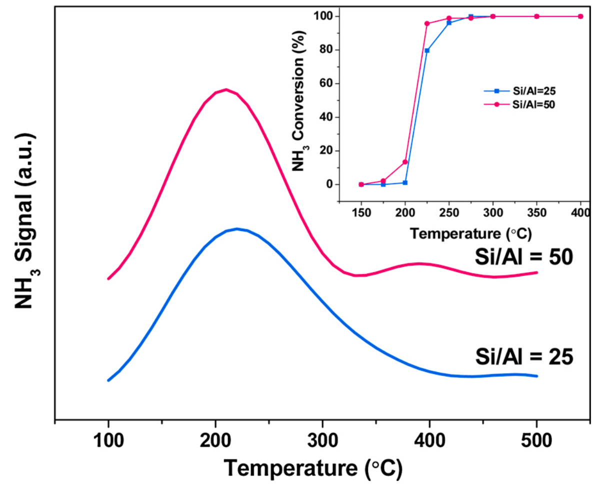

Fig. 7. NH_3-TPD and NH_3 conversion (inset) at different temperatures over Pt-Fe/ZSM-5 (Si/Al ratio 25 and 50) samples after hydrothermal aging. Reaction conditions: $[NH_3] = 500$ ppm, $[O_2] = 10$ %, $[H_2O] = 5$ %, balance N_2, total flow ratio = 100 mL/min, GHSV = 140,000 h^{-1}.

3.2.3. Acid sites

The surface acid properties of the catalysts were studied by NH_3-TPD experiments and the results are shown in Fig. 6. Similar asymmetric peaks can be observed on the Pt-Fe/ZSM-5 samples, indicating the existence of acid sites with different strength [27]. It can be observed in Fig. 6 that the total peak area (T_{area}) of NH_3-TPD for Pt-Fe/ZSM-5 (Si/Al = 25) was bigger than that of Pt-Fe/ZSM-5 (Si/Al = 50), indicated that Pt-Fe/ZSM-5 (Si/Al = 25) sample possessed more acid sites than Pt-Fe/ZSM-5 (Si/Al = 50) sample. The overlapped peaks were then fitted and separated into four sub-bands located at around 80 ℃, 120 ℃, 200 ℃ and 350 ℃, which can be assigned to physisorbed NH_3, NH_3 bound to weak, medium and strong acid sites [56,57], respectively. It can be observed in the Fig. 6 that weak and medium acid sites were the main existence form for Pt-Fe/ZSM-5 (Si/Al = 25), while strong acid sites were dominating in Pt-Fe/ZSM-5 (Si/Al = 50). Combined with the high water-resisting property on Pt-Fe/ZSM-5 (Si/Al = 50) in Fig. 1, it could be concluded that this water-resisting property might be related to the strong acid sites of Pt-Fe/ZSM-5 (Si/Al = 50) catalyst.

In order to further prove the necessity of strong acid sites for the water-resisting property of the catalysts during NH_3-SCO with H_2O adding, the strong acid sites were removed through hydrothermal aging at 700 ℃ reported by Riguetto [58]. The NH_3-TPD results in Fig. 7 verified that after hydrothermal aging the content of strong acid sites over Pt-Fe/ZSM-5 (Si/Al 25) and Pt-Fe/ZSM-5 (Si/Al 50) decreased dramatically to zero. As we speculated above, when the strong acid sites over the NH_3-SCO catalysts were removed, the NH_3-SCO activity of the samples decreased accordingly, more than 30 % decrease of NH_3 conversion can be observed on both samples (shown in Fig. 7 insert). Therefore, strong acid sites were necessary for the water-resisting property of the catalysts during NH_3-SCO with H_2O adding.

Ammonia adsorption in both the presence and absence of water was studied through *in situ* DRIFTS over Pt-Fe/ZSM-5 (Si/Al = 25 and 50) samples to confirm the role of acid sites in water-resisting property. The adsorption experiment was conducted at 100 ℃ for 1 h, when the adsorption had reached steady state. As presented in Fig. 7, various peaks were observed after NH_3 adsorption saturation. The negative bands located at 3500−3710 cm^{-1} were assigned to the consumption of OH groups due to the interaction of surface hydroxyls with NH_3 [36,47]. The other peaks appeared in the range of 3500−1400 cm^{-1} were the vibration of adsorbed NH_3 species [36]. It can be observed that the intensity of adsorbed ammonia species over Pt-Fe/ZSM-5 (Si/Al = 25) was stronger than that on Pt-Fe/ZSM-5 (Si/Al = 50) in dry circumstance, which might result from the larger surface area (Fig. 1) and more weak and medium acid sites of Pt-Fe/ZSM-5 (Si/Al = 25). With the addition of H_2O (wet circumstance), the intensity of NH_3 species decreased dramatically on both samples, however, the strength was reversed on the two samples. More NH_3 species was adsorbed on Pt-Fe/ZSM-5 (Si/Al = 50) than Pt-Fe/ZSM-5 (Si/Al = 25), which should be due to the strong acid sites of Pt-Fe/ZSM-5 (Si/Al = 50) catalyst (Fig. 8).

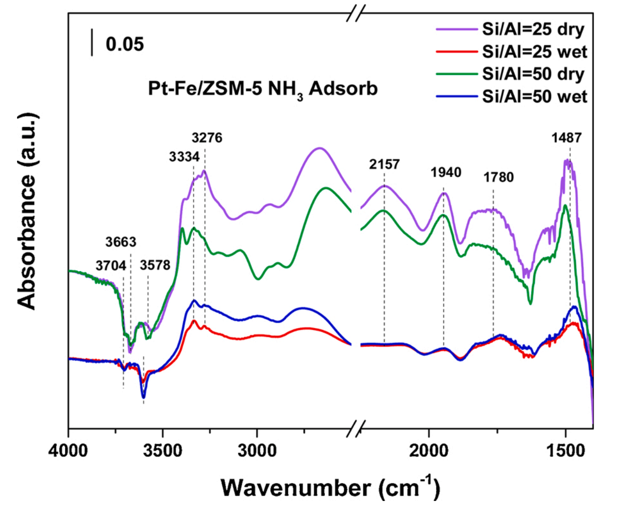

Fig. 8. *in situ* DRIFTS of NH_3 adsorption at 100 ℃ for 30 min in dry and wet circumstances. Reaction conditions: $[NH_3] = 500$ ppm, $O_2 = 10$ %, $H_2O = 5$% (when added) and N_2 balance.

3.3. Results of DFT calculation

DFT calculations were then carried out to investigate the influence of acid site on H_2O and NH_3 adsorption on ZSM-5 samples. Firstly, we constructed two types of ZSM-5 structures, one is ZSM-5 (Fig. 9a) without extra acid sites added, NH_3 mainly adsorbed on the L acid sites or by weak adsorption. According to the literature [58], Brønsted acid sites were much stronger than L acid sites. Thus, in this work a H atom was inserted on ZSM-5 structure (denoted as ZSM-5-H) to imitate Brønsted acid site in the other structure (Fig. 9b). The adsorption configurations of H_2O and NH_3 on ZSM-5 and ZSM-5-H were optimized and the corresponding adsorption energies were calculated (Fig. 9c–f). The results showed that all of the adsorption energies had negative values, indicating that both of ZSM-5 and ZSM-5-H had affinity for H_2O and NH_3. In addition, the adsorption intensity of H_2O and NH_3 increased dramatically (about 5 times higher) when Brønsted acid site was involved. Remarkably, the adsorption of H_2O was slightly superior to NH_3 on weak adsorption sites for ZSM-5, which will definitely result in the competitive adsorption during NH_3-SCO in wet circumstance. However, the adsorption energy of NH_3 was much lower than H_2O (0.31 eV) when strong acid site was introduced, indicated that strong acid sites induced NH_3 to dominate in the competitive adsorption with H_2O. This result was highly consistent with data obtained through *in situ* DRIFTS and NH_3-TPD mentioned above.

4. Conclusion

Pt-Fe/ZSM-5 catalysts with different Si/Al ratio (25 and 50) were prepared in this work and the NH_3-SCO activity were compared both in dry and wet (5% H_2O) circumstance. Characterization results showed that abundant metallic Pt (Pt°) was beneficial for Si/Al 25 sample to exhibit higher intrinsic NH_3-SCO activity (in dry circumstance). After H_2O adding, the activity of Si/Al 25 sample decreased dramatically while the activity of Si/Al 50 sample maintained much higher level. It was found through NH_3-TPD that strong acid site was dominating in Si/Al 50 sample. *In situ* DRIFTS and DFT calculation results finally

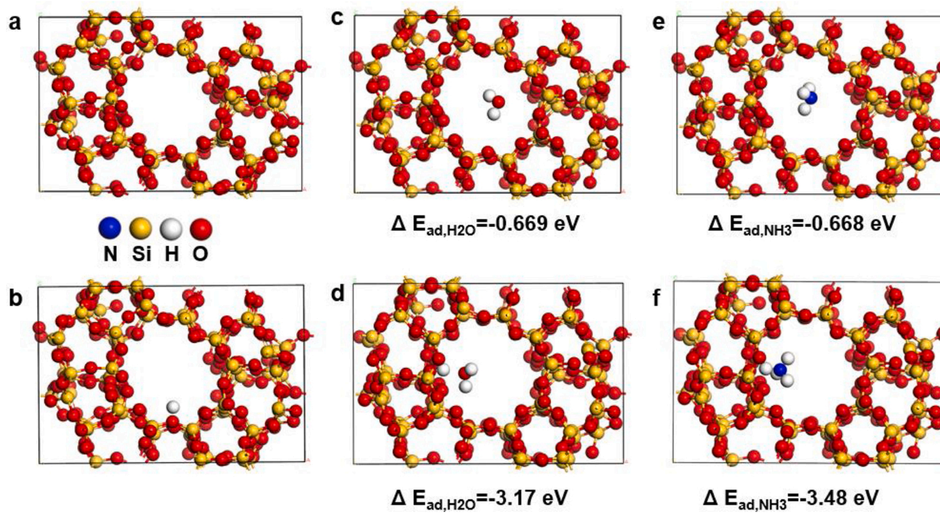

Fig. 9. Optimized structures of (a) ZSM-5 and (b) ZSM-5-H (acid site), possible adsorption configurations of (c) H_2O and (e) NH_3 on ZSM-5 and (d) H_2O and (f) NH_3 on ZSM-5-H (acid site). Color code: blue (N), yellow (Si), white (H), red (O). (For interpretation of the references to colour in this figure legend, the reader is referred to the web version of this article).

confirmed that the competitive adsorption between H_2O and NH_3 inhibited the NH_3-SCO activity in wet circumstance, while acid sites induced NH_3 to dominate in the competitive adsorption with H_2O. Thus, due to the dominating of strong acid sites, Pt-Fe/ZSM-5 (Si/Al 50) catalyst maintained higher NH_3-SCO activity when H_2O was introduced compared to Pt-Fe/ZSM-5 (Si/Al 25), which is a potential catalyst of selective ammonia oxidation in diesel vehicles exhaust gas purification system.

CRediT authorship contribution statement

Fei Wang: Conceptualization, Formal analysis, Funding acquisition, Writing - original draft. **Ying Zhu:** Data curation, Investigation. **Zhao Li:** Methodology, Validation. **Yulong Shan:** Formal analysis. **Wenpo Shan:** Supervision. **Xiaoyan Shi:** Conceptualization. **Yunbo Yu:** Funding acquisition, Formal analysis. **Changbin Zhang:** Methodology, Validation. **Kai Li:** Supervision. **Ping Ning:** Project administration. **Yan Zhang:** Funding acquisition, Writing - review & editing. **Hong He:** Funding acquisition, Writing - review & editing.

Declaration of Competing Interest

The authors declare no competing financial interest.

Acknowledgements

This work was financially supported by the National Key R&D Program of China (2017YFC0211105), National Natural Science Foundation of China (51908532) and the Chinese Postdoctoral Science Foundation (2019M663911XB).

Appendix A. Supplementary data

Supplementary material related to this article can be found, in the online version, at doi:https://doi.org/10.1016/j.cattod.2020.06.039.

References

[1] Y. Pan, S. Tian, D. Liu, Y. Fang, X. Zhu, Q. Zhang, B. Zheng, G. Michalski, Y. Wang, Fossil fuel combustion-related emissions dominate atmospheric ammonia sources during severe haze episodes: evidence from ^{15}N-stable isotope in size-resolved aerosol ammonium, Environ. Sci. Technol. 50 (2016) 8049–8056.

[2] S.N. Behera, M. Sharma, V.P. Aneja, R. Balasubramanian, Ammonia in the atmosphere: a review on emission sources, atmospheric chemistry and deposition on terrestrial bodies, Environ. Sci. Pollut. Res. - Int. 20 (2013) 8092–8131.

[3] J. Turšič, A. Berner, B. Podkrajšek, I. Grgić, Influence of ammonia on sulfate formation under haze conditions under haze conditions, Atmos. Environ. 38 (2004) 2789–2795.

[4] R.Z. Gehui Wang, Mario E. Gomez, Lingxiao Yang, Misti Levy Zamora, Hu Min, Yun Lin, Jianfei Peng, Song Guo, Jingjing Meng, Jianjun Li, Chunlei Cheng, Hu Tafeng, Yanqin Ren, Yuesi Wang, Jian Gao, Junji Cao, Zhisheng An, Weijian Zhou, Guohui Li, Jiayuan Wang, Pengfei Tian, Wilmarie Marrero-Ortiz, Jeremiah Secrest, Du Zhuofei, Jing Zheng, Dongjie Shang, Limin Zeng, Min Shao, Weigang Wang, Yao Huang, Yuan Wang, Yujiao Zhu, Yixin Li, Hu Jiaxi, Bowen Pan, Cai Li, Yuting Cheng, Yuemeng Ji, Fang Zhang, Daniel Rosenfeld, Peter S. Liss, Robert A. Duce, Charles E. Kolb, Mario J. Molina, Persistent sulfate formation from London Fog to Chinese haze, Proc. Natl. Acad. Sci. U. S. A. 113 (2016) 13630–13635.

[5] B. Chu, X. Zhang, Y. Liu, H. He, Y. Sun, J. Jiang, J. Li, J. Hao, Synergetic formation of secondary inorganic and organic aerosol: effect of SO_2 and NH_3 on particle formation and growth, Atmos. Chem. Phys. 16 (2016) 14219–14230.

[6] K. Sun, L. Tao, D.J. Miller, D. Pan, L.M. Golston, M.A. Zondlo, R.J. Griffin, H. W. Wallace, Y.J. Leong, M.M. Yang, Y. Zhang, D.L. Mauzerall, T. Zhu, Vehicle emissions as an important urban ammonia source in the United States and China, Environ. Sci. Technol. 51 (2017) 2472–2481.

[7] T. Zhang, H. Chang, Y. You, C. Shi, J. Li, Excellent activity and selectivity of one-pot synthesized Cu-SSZ-13 catalyst in the selective catalytic oxidation of ammonia to nitrogen, Environ. Sci. Technol. 52 (2018) 4802–4808.

[8] L. Zhang, C. Zhang, H. He, The role of silver species on Ag/Al_2O_3 catalysts for the selective catalytic oxidation of ammonia to nitrogen, J. Catal. 261 (2009) 101–109.

[9] S. Hong, A. Karim, T.S. Rahman, K. Jacobi, G. Ertl, Selective oxidation of ammonia on RuO_2(110): a combined DFT and KMC study, J. Catal. 276 (2010) 371–381.

[10] X. Lu, Z. Deng, K.-S. Chau, L. Li, Z. Wen, W. Guo, C.-M.L. Wu, Mechanistic insight into catalytic oxidation of ammonia on clean, O- and OH-assisted Ir(1 1 1) surfaces, ChemCatChem 5 (2013) 1832–1841.

[11] C.-C. Wang, J.-Y. Wu, T.L.M. Pham, J.-C. Jiang, Microkinetic simulation of ammonia oxidation on the RuO_2(110) surface, ACS Catal. 4 (2014) 639–648.

[12] J. Gong, R.A. Ojifinni, T.S. Kim, J.M. White, C.B. Mullins, Selective catalytic oxidation of ammonia to nitrogen on atomic oxygen precovered Au(111), J. Am. Chem. Soc. 128 (2006) 9012–9013.

[13] C.-M. Hung, Cordierite-supported Pt–Pd–Rh ternary composite for selective catalytic oxidation of ammonia, Powder Technol. 200 (2010) 78–83.

[14] J. Fu, K. Yang, C. Ma, N. Zhang, H. Gai, J. Zheng, B.H. Chen, Bimetallic Ru–Cu as a highly active, selective and stable catalyst for catalytic wet oxidation of aqueous ammonia to nitrogen, Appl. Catal. B 184 (2016) 216–222.

[15] M. Amblard, R. Burch, B.W.L. Southward, A study of the mechanism of selective conversion of ammonia to nitrogen on Ni gamma Al_2O_3 under strongly oxidising conditions, Catal. Today 59 (2000) 365–371.

[16] T. Curtin, F.O. Regan, C. Deconinck, N. Knüttle, B.K. Hodnett, The catalytic oxidation of ammonia influence of water and sulfur on selectivity to nitrogen over promoted copper oxide alumina catalysts, Catal. Today 55 (2000) 189–195.

[17] R.Q. Long, R.T. Yang, Selective catalytic oxidation of ammonia to nitrogen over Fe_2O_3–TiO_2 prepared with a Sol-Gel method, J. Catal. 207 (2002) 158–165.

[18] R.-M. Yuan, G. Fu, X. Xu, H.-L. Wan, Mechanisms for selective catalytic oxidation of ammonia over vanadium oxides, J. Phys. Chem. C 115 (2011) 21218–21229.

[19] L. Gang, J. van Grondelle, B.G. Anderson, R.A. van Santen, Selective low temperature NH_3 oxidation to N_2 on copper-based catalysts, J. Catal. 186 (1999) 100–109.

[20] L. Chmielarz, P. Kuśtrowski, A. Rafalska-Łasocha, R. Dziembaj, Selective oxidation of ammonia to nitrogen on transition metal containing mixed metal oxides, Appl. Catal. B 58 (2005) 235–244.
[21] M. Jabłońska, R. Palkovits, Copper based catalysts for the selective ammonia oxidation into nitrogen and water vapour-Recent trends and open challenges, Appl. Catal. B 181 (2016) 332–351.
[22] P. Li, R. Zhang, N. Liu, S. Royer, Efficiency of Cu and Pd substitution in Fe-based perovskites to promote N_2 formation during NH_3 selective catalytic oxidation (NH_3-SCO), Appl. Catal. B 203 (2017) 174–188.
[23] R.Q. Long, R.T. Yang, Superior ion-exchanged ZSM-5 catalysts for selective catalytic oxidation of ammonia to nitrogen, Chem. Commun. 0 (2000) 1651–1652.
[24] R.Q. Long, R.T. Yang, Noble metal (Pt, Rh, Pd) promoted Fe-ZSM-5 for selective catalytic oxidation of ammonia to N_2 at low temperatures, Catal. Lett. 78 (2002) 353–357.
[25] M. Jabłońska, A. Król, E. Kukulska-Zajac, K. Tarach, L. Chmielarz, K. Góra-Marek, Zeolite Y modified with palladium as effective catalyst for selective catalytic oxidation of ammonia to nitrogen, J. Catal. 316 (2014) 36–46.
[26] S. Heylen, N. Delcour, C.E.A. Kirschhock, J.A. Martens, Selective catalytic oxidation of Ammonia into Dinitrogen over a zeolite-supported ruthenium dioxide catalyst, ChemCatChem 4 (2012) 1162–1166.
[27] A. Akah, C. Cundy, A. Garforth, The selective catalytic oxidation of NH_3 over Fe-ZSM-5, Appl. Catal. B 59 (2005) 221–226.
[28] J. Guo, Y. Peng, Y. Zhang, W. Yang, L. Gan, K. Li, J. Chen, J. Li, Comparison of NH_3-SCO performance over CuOx/H-SSZ-13 and CuOx/H-SAPO-34 catalysts, Appl. Catal. A Gen. 585 (2019), 117119.
[29] J. Guo, W. Yang, Y. Zhang, L. Gan, C. Fan, J. Chen, Y. Peng, J. Li, A multiple-active-site Cu/SSZ-13 for NH_3-SCO: influence of Si/Al ratio on the catalytic performance, Catal. Commun. 135 (2020) 105751.
[30] E. Kolobova, A. Pestryakov, G. Mamontov, Y. Kotolevich, N. Bogdanchikova, M. Farias, A. Vosmerikov, L. Vosmerikova, V. Cortes Corberan, Low-temperature CO oxidation on Ag/ZSM-5 catalysts: influence of Si/Al ratio and redox pretreatments on formation of silver active sites, Fuel 188 (2017) 121–131.
[31] F. Wang, J. Ma, G. He, M. Chen, C. Zhang, H. He, Nanosize effect of Al_2O_3 in Ag/Al_2O_3 catalyst for the selective catalytic oxidation of ammonia, ACS Catal. 8 (2018) 2670–2682.
[32] J. Liu, Q. Lin, S. Liu, S. Xu, H. Xu, Y. Chen, Promotional effects of ascorbic acid on the low-temperature catalytic activity of selective catalytic oxidation of ammonia over Pt/SA: effect of Pt° content, New J. Chem. 44 (2020) 4108–4113.
[33] B. Xing, J. Ma, R. Li, H. Jiao, Location, distribution and acidity of Al substitution in ZSM-5 with different Si/Al ratios – a periodic DFT computation, Catal. Sci. Technol. 7 (2017) 5694–5708.
[34] G. Qi, J.E. Gatt, R.T. Yang, Selective catalytic oxidation (SCO) of ammonia to nitrogen over Fe-exchanged zeolites prepared by sublimation of $FeCl_3$, J. Catal. 226 (2004) 120–128.
[35] S. Shrestha, M.P. Harold, K. Kamasamudram, A. Yezerets, Selective oxidation of ammonia on mixed and dual-layer Fe-ZSM-5+Pt/Al_2O_3 monolithic catalysts, Catal. Today 231 (2014) 105–115.
[36] G. Qi, R.T. Yang, Selective catalytic oxidation (SCO) of ammonia to nitrogen over Fe/ZSM-5 catalysts, Appl. Catal. A Gen. 287 (2005) 25–33.
[37] F. Wang, J. Ma, G. He, M. Chen, S. Wang, C. Zhang, H. He, Synergistic effect of TiO_2–SiO_2in Ag/Si–Ti catalyst for the selective catalytic oxidation of ammonia, Ind. Eng. Chem. Res. 52 (2018) 11903–11910.
[38] J.P. Perdew, K. Burke, M. Ernzerhof, Generalized gradient approximation made simple, Phys. Rev. Lett. 77 (1996) 3865–3868.
[39] S. Grimme, S. Ehrlich, L. Goerigk, Effect of the damping function in dispersion corrected density functional theory, J. Comput. Chem. 32 (2011) 1456–1465.
[40] G. Kresse, J. Furthmüller, Efficient iterative schemes for ab initio total-energy calculations using a plane-wave basis set, Phys. Rev. B 54 (1996) 11169–11186.
[41] G. Kresse, D. Joubert, From ultrasoft pseudopotentials to the projector augmented-wave method, Phys. Rev. B 59 (1999) 1758–1775.
[42] S.M. Opalka, T. Zhu, Influence of the Si/Al ratio and Al distribution on the H-ZSM-5 lattice and Brønsted acid site characteristics, Microporous Mesoporous Mater. 222 (2016) 256–270.
[43] H. Sjövall, R.J. Blint, L. Olsson, Detailed kinetic modeling of NH_3 and H_2O adsorption, and NH_3 oxidation over Cu-ZSM-5, J. Phys. Chem. C 113 (2009) 1393–1405.
[44] A. López, I. de Marco, B.M. Caballero, M.F. Laresgoiti, A. Adrados, A. Aranzabal, Catalytic pyrolysis of plastic wastes with two different types of catalysts: ZSM-5 zeolite and Red Mud, Appl. Catal. B 104 (2011) 211–219.
[45] Y. Tao, H. Kanoh, K. Kaneko, ZSM-5 monolith of uniform mesoporous channels, J. Am. Chem. Soc. 125 (2003) 6044–6045.
[46] C. Zhang, Q. Liu, Z. Xu, et al., Synthesis and characterization of composite molecular sieves with mesoporous and microporous structure from ZSM-5 zeolites by heat treatment, Microporous Mesoporous Mater. 62 (2003) 157–163.
[47] X. Shi, F. Liu, L. Xie, W. Shan, H. He, NH3-SCR performance of fresh and hydrothermally aged Fe-ZSM-5 in standard and fast selective catalytic reduction reactions, Environ. Sci. Technol. 47 (2013) 3293–3298.
[48] M.S. Kumar, D. Chen, J.C. Walmsley, et al., Dehydrogenation of propane over Pt-SBA-15: effect of Pt particle size, Catal. Commun. 9 (2008) 747–750.
[49] M.S. Kumar, D. Chen, A. Holmen, et al., Dehydrogenation of propane over Pt-SBA-15 and Pt-Sn-SBA-15: effect of Sn on the dispersion of Pt and catalytic behavior, Catal. Today 142 (2009) 17–23.
[50] B.A. Riguetto, S. Damyanova, G. Gouliev, C.M.P. Marques, L. Petrov, J.M.C. Bueno, Surface behavior of alumina-supported Pt catalysts modified with cerium as revealed by X-ray diffraction, X-ray photoelectron spectroscopy, and fourier transform infrared spectroscopy of CO adsorption, J. Phys. Chem. B 108 (2004) 5349–5358.
[51] J.C. Serrano-Ruiz, G.W. Huber, M.A. Sánchez-Castillo, et al., Effect of Sn addition to Pt/CeO_2–Al_2O_3 and Pt/Al_2O_3 catalysts: an XPS, 119 Sn Mössbauer and microcalorimetry study, J. Catal. 241 (2006) 378–388.
[52] Y. Yan, S. Jiang, H. Zhang, X. Zhang, Preparation of novel Fe-ZSM-5 zeolite membrane catalysts for catalytic wet peroxide oxidation of phenol in a membrane reactor, Chem. Eng. J. 259 (2015) 243–251.
[53] R.Q. Long, R.T. Yang, Characterization of Fe-ZSM-5 catalyst for selective catalytic reduction of nitric oxide by Ammonia, J. Catal. 194 (2000) 80–90.
[54] N. An, Q. Yu, G. Liu, S. Li, M. Jia, W. Zhang, Complete oxidation of formaldehyde at ambient temperature over supported Pt/Fe_2O_3 catalysts prepared by colloid-deposition method, J. Hazard. Mater. 186 (2011) 1392–1397.
[55] Y.-S. Shi, Z.-F. Yuan, Q. Wei, K.-Q. Sun, B.-Q. Xu, Pt–FeOx/SiO_2 catalysts prepared by galvanic displacement show high selectivity for cinnamyl alcohol production in the chemoselective hydrogenation of cinnamaldehyde, Catal. Sci. Technol. 6 (2016) 7033–7037.
[56] Y. Peng, C. Liu, X. Zhang, J. Li, The effect of SiO_2 on a novel CeO_2–WO_3/TiO_2 catalyst for the selective catalytic reduction of NO with NH_3, Appl. Catal. B 140–141 (2013) 276–282.
[57] F. Arena, R. Dario, A. Parmaliana, A characterization study of the surface acidity of solid catalysts by temperature programmed methods, Appl. Catal. A Gen. 170 (1998) 127–137.
[58] Y. Shan, X. Shi, Z. Yan, J. Liu, Y. Yu, H. He, Deactivation of Cu-SSZ-13 in the presence of SO_2 during hydrothermal aging, Catal. Today 320 (2019) 84–90.